

AN EXPERIMENTAL SIMULATION ON THE INFLUENCE OF DIFFERENT FILM COOLING HOLE SHAPES ON PARTICLE DEPOSITION ON TURBINE VANE

Zhengang Liu¹, Rongsheng Ruan¹, Long Cheng¹, Yixuan Zhang¹, Zhenxia Liu¹& Dingyi Wu¹

¹ School of Power and Energy, Northwestern Polytechnical University, Xi'an, China, 710072

Abstract

The deposition of particles, such as sands, dusts and volcanic ashes, on turbines could reduce the aerodynamic and cooling performance of turbines. To investigate the effect of film-cooling with different holes shapes on the deposition, an experiment at about ambient temperature is designed, in which the test models are plates but with different film-cooling hole shapes and a kind of wax is atomized as the particles. Firstly, the influence of angle of attack (AOA) on deposition is studied. The results show that, under different AOAs, the deposition rates on the pressure surface increase with the increase of AOAs. As the AOA increases from 0° to -15°, the relative increase in the deposition rate on the pressure surface of the cylindrical model is 110%, however, the deposition distribution does not change much. Therefore, the angle of attack is selected as -5° for research on the different hole shapes. After this, the effect of different hole shapes on deposition is also studied. The results show that the fan-shaped film-cooling hole could reduce the deposition rate 83% than the cylindrical film-cooling holes, and the RTSH film-cooling hole could reduce the deposition rate 79%, although most deposition forms near the film-cooling holes for all film-cooling holes shapes. The film-cooling efficiency of the plate with the fan-shaped hole could be improved by up to 16% (not relative value), and the RTSH filmcooling hole could be improved by up to 29% (not relative value), although the film-cooling efficiencies for all film-cooling holes shapes are not changed dramatically by the deposition under the experimental conditions. This study may be helpful for developing the technology of reducing the deposition and its harm on turbines.

Keywords: particle deposition; hole shapes; deposition rate; cooling effectiveness; angle of attack.

1. General Introduction

When aircrafts fly in environments with high concentrations of sand, dust, and other particles, the engines will inhale a large number of these particles. After entering the aero engine, these particles undergo heating in the combustion chamber and then interact with the turbine vanes in a molten or solid-state, depositing on the surface of the turbine vanes. This affects the aerodynamic and heat transfer characteristics of the turbine vanes and may even block the film cooling holes, leading to the erosion of the turbine vanes and accordingly a flight accident.

Experimental research on the particle deposition on turbine vanes mainly consists of two types: high-temperature deposition studies, where the mainstream temperature is close to the actual temperature in front of the turbine, and ambient temperature deposition studies, where the mainstream temperature is slightly higher than room temperature. Jenson et al. [1] developed the Turbine Accelerated Deposition Facility (TADF) specifically to simulate the deposition process on turbine vanes, thereby facilitating rapid testing that can replicate the accumulation of particles on turbine vanes within four hours, equivalent to thousands of hours of actual operational conditions. Smith et al. [2] developed the Turbine Reacting Flow Rig (TuRFR), featuring vane passage channels, to enable real-time measurements of the surface temperature of the test model.

Meanwhile, Prenter et al. [3] conducted research exploring the impact of unequal inlet gas temperature distribution on particle deposition, revealing that regions with higher temperatures tend to experience greater deposition rates. Liu et al. [4-5] designed a high temperature deposition test platform to study the influence of mainstream gas temperature and transverse trench structures on the deposition of particles. They found that when the gas temperature approached the melting point of the particles, the deposition rate increased significantly. The introduction of transverse trenches significantly suppressed particle deposition on the vane surface. As the trench depth increased, a noticeable reduction in deposition was observed in the area downstream of the film cooling holes. Given the complexities involved in high-temperature testing, scholars have begun exploring ambient temperature deposition experiments, utilizing similarity theory as a foundation, to gain a deeper understanding of deposition characteristics. Lawson et al. [6-8] developed an ambient temperature deposition test platform, utilizing wax as the particulate phase for their study. Their findings showed that as wax deposition accumulated, the film cooling efficiency gradually diminished. Furthermore, they observed that an elevation in the blowing ratio further intensified the adverse effects of deposition on the vane surface cooling. Expanding upon previous research, Albert et al. [9] constructed an ambient temperature deposition test platform, with a recirculating low-speed closed-loop wind tunnel serving as its core component. Following a similar approach, they emulated particle deposition by utilizing wax and observed that the wax tended to accumulate in bulky formations, in some cases even obstructing the film cooling holes positioned at the vane's leading edge. Albert et al. [10] delved deeper into the impact of transverse trench structures on deposition and discovered fascinating insights. Their study revealed that, in contrast to cylindrical film cooling holes, trenched structures indeed prompted particle deposition within the trenches. However, interestingly, the downstream deposition distribution exhibited a more uniform pattern. Davidson et al. [11] studied the impact of four film cooling hole configurations on the deposition, including cylindrical holes, dimpled holes, transverse trenches, and modified trenches. The results indicated that the presence of film cooling significantly exacerbated the deposition. Furthermore, the study by Davidson et al. [11] demonstrated that, in comparison to cylindrical film cooling holes, dimpled holes and transverse trenches exhibited superior performance in reducing particle deposition downstream of the film cooling holes. Liu et al. [12-13] conducted a study in a low-speed wind tunnel to investigate the influence of film cooling and transverse trenches on the deposition. They found that the film cooling structures significantly increases the particles deposition on the flat plate surface, particularly downstream of the film cooling holes. Additionally, Liu et al. [12-13] found that the transverse trench configuration leads to a more uniform distribution of deposition downstream of the film cooling holes. This feature not only enhances deposition control but also contributes to reduced wax deposition. Yang et al. [14-15] constructed a low-speed open-loop wind tunnel to meticulously investigate the deposition patterns on film-cooled flat plate surfaces. Their findings revealed an intriguing trend: as the blowing ratio rose from 0 to 1.5, deposition initially decreased but then showed an upward trend.

Currently, film cooling is used on most high-performance turbine vanes to protect the vanes from being heated. However, the presence of film cooling causes interference between the mainstream and cooling flows, which seriously affects the deposition characteristics of particles on the vane surface. Changes in the film cooling hole shape not only affect the cooling efficiency of the vane but also the flow field structure behind the film cooling hole, which in turn affects the movement and heat transfer of particles in the flow field, leading to changes in the amount and distribution of particle deposition on the vane surface.

In this paper, cylindrical holes, RTSH holes, and fan-shaped holes have been selected as the focal research objects for conducting ambient temperature particle deposition experiments. Furthermore, we have also examined the impact of the angle of attack (AOA) on deposition patterns. The study aims to delve into the intricate influence of film cooling hole shapes on particle deposition under various operating conditions. By doing so, we hope to gain profound insights into the deposition mechanisms at play and provide valuable guidance for the effective protection of

turbine vanes against particle deposition.

2. Experimental System and Parameters

2.1 Experimental facilities

The experimental system applied by Liu et al [12] and consists of the wind tunnel, the wax spray system and the cooling air system, however, the last of which is revised. The experimental scheme is shown in Figure 1. A kind of wax is used for simulating the particles in harsh environments, and the film-cooled flat plate serves as the test model. The wax deposition on the flat plate surface simulates the deposition of particles on the actual turbine blade surface. The airflow in the wind tunnel is heated by a heater and then mixed with atomized particles after passing through a turbulent generator, forming a sparse multiphase flow. When the particles in the airflow collide with the test model, some will deposit on the surface of the test model. After the experiment, the deposition morphology and distribution are captured using a camera, and the mass of the deposited wax is measured using a high-precision balance.

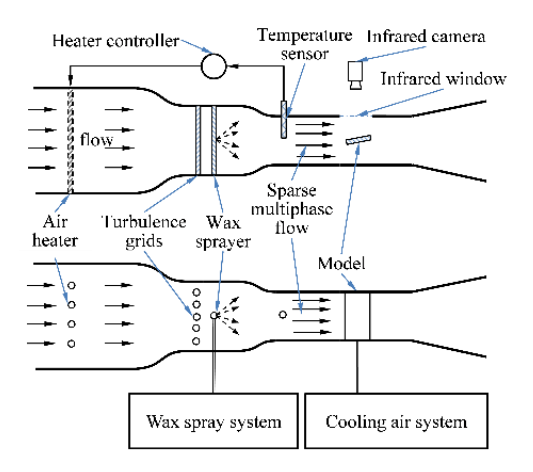


Figure 1-Experimental schematic

Firstly, two important parameters are introduced here for the following discussion. The first one is the deposition rate β of the wax particles on the model surface, which is defined as the ratio of the mass of particles m_{dep} deposited on the test model surface to the total mass m_{total} of wax particles injection:

$$\beta = \frac{m_{dep}}{m_{total}} \tag{1}$$

In addition to the deposition rate, reflecting the amount of the deposition, the deposition distribution is also concerned and discussed.

The second parameter associated with the cooling performance and is cooling efficiency. It is a dimensionless parameter and defined as

$$\eta = \frac{T_{\infty} - T_{w}}{T_{\infty} - T_{c}} \tag{2}$$

where T_{∞} is the mainstream temperature, T_w is the surface temperature of the model and T_c is the temperature of the cooling air. Obviously, the cooling efficiency is associated with the surface temperature. Under the same condition, the higher surface temperature means lower cooling efficiency, and lower surface temperature means higher cooling efficiency.

2.2 Testing models

In this study, all test models consist of the dimensional plates, but with varying film cooling

setups. The referred model, depicted in Figure 2, which has the dimensions 200mm (length)×308mm (width)×30mm (height). The leading edge has a semi-circular chamfer with a diameter of 30mm. The upper surface of the plate is equipped with 21 film cooling holes, each with a diameter of 2mm, spaced 3mm apart in the spanwise direction, and with a backward inclined angle at 30° (as shown in Figure 3). The film cooling holes are connected to the internal cavity of the model. During the experiment, the cooling air enters the cavity from the cooling air inlet channel of the model (as shown in Figure 2 (a)), then flows out from the cavity and enters the mainstream through the film cooling holes to simulate the film cooling of turbine vanes. Additionally, three thermocouples are embedded on the upper surface for calibrating the infrared camera. The model surface is black to reduce errors caused by the infrared camera.



Figure 2–Testing models

Figure 3 shows two types of film-cooling hole selected for the experiment, in addition to the cylindrical hole. All dimensions in the figure are in millimeter. The models for all hole shapes are designed with a minimum throat area of πmm^2 of the film-cooling hole. The paper focuses on three different film-cooling hole shapes: cylindrical, fan-shaped, and RTSH film-cooling holes. For the convenience of discussion, the three models are called as cylindrical, conical and CONSOLE model, respectively.

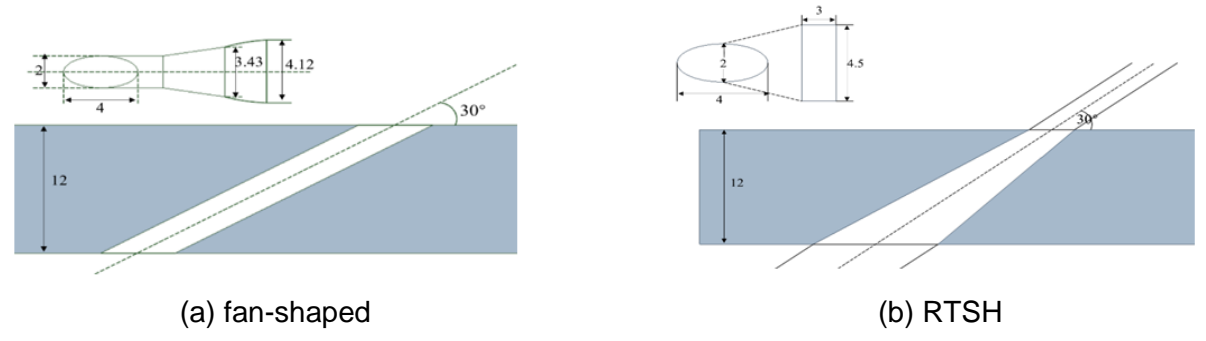


Figure 3-Film cooling hole geometry dimension

Figure 4 illustrates how the model is fixed in the test section channel. The width of the model is equal to the width of the test section to minimize the influence of the edges. The AOA (α) of the model could be adjusted by rotating the discs, as shown in Figure 4. In this paper, as shown in Figure 5, all the AOAs are negative and as a result, the upper surface of the model is the pressure surface (PS) while the lower surface is the suction surface.

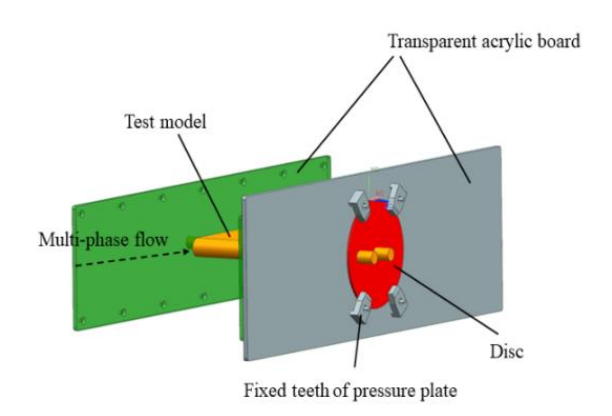


Figure 4-Fixation of experimental pieces

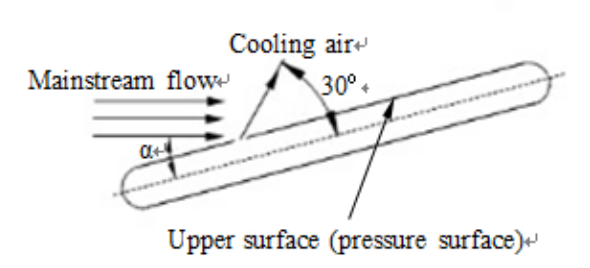


Figure 5–Schematic of multiphase flow and angle of attack

2.3 Experimental parameters

The primary variables of the experiment are outlined in Table 1. Wax is maintained at a constant flow rate of 15g/min, and a laser particle size analyzer is employed to obtain the particle size distribution at this specific flow rate, as illustrated in Figure 6. Predominantly, the wax particles range from 5 to 20 µm in size, with an approximate average diameter of 10µm. The Stokes number is one important parameter of determining the trajectory of these particles and defined as follows:

$$St = \frac{\rho_p d_p^2 \nu_\infty}{18\mu_\infty L} \tag{3}$$

where ρ_p represents particle density, d_p is particle diameter, u_∞ is the mainstream flow velocity, L is the characteristic length, and μ_∞ is flow dynamic viscosity. The physical meaning of St is the ratio of the particle relaxation time to the fluid characteristic time, also the comparison between particle inertia and diffusion effect, namely, a smaller St indicates lower particle inertia, better flow tracking, and that the diffusion effect play more role in the particle trajectory.

Taking the model length, i.e. the streamwise length, as shown in Figure 2(a)), as the characteristic length (0.2m), with wax density ρ_p =880kg/m³ and flow dynamic viscosity μ_{∞} =1.7984×10-5kg/(m·s), the calculated St is approximately in the range of 0.003 to 0.054, which means that the wax particles could diffuse in the mainstream flow uniformly enough.

Table 1 The main experimental parameters

Wax temperature(K)	Mainstream velocity <i>u</i> ∞ (m/s)	Mainstream temperature T_{∞} (K)	Cooling air temperature $T_c(K)$	AOA α(°)	Blow ratio <i>M</i>	Test time (min)	Wax mass flow rate (g/min)
333	10	313	278	-15~0	3	3	15

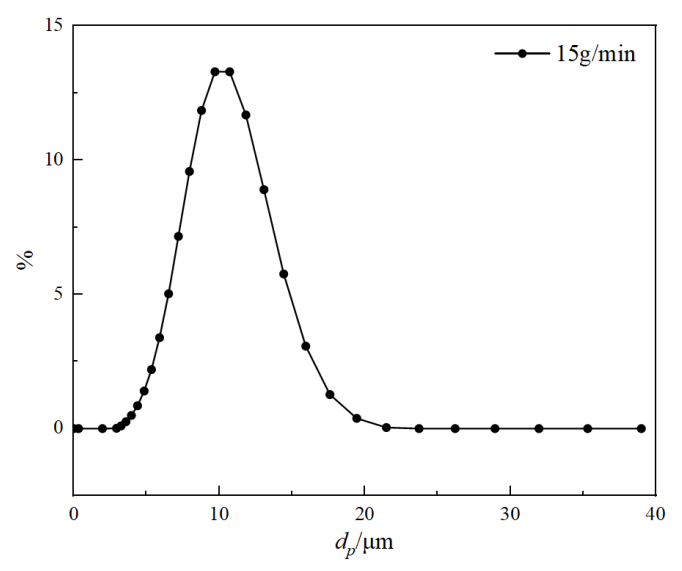


Figure 6-Wax particle size distribution

3. Result and Discussion

3.1 Uncertainty Analysis

The measurement errors of the experimental system affect the accuracy and reliability of the tests. Therefore, before conducting the formal experiment, five tests under the same condition were conducted on the model to measure the deposition mass of wax pressure surface (PS) of the model and followed by error analysis. The uncertainty of the experimental measurement (Δm_{dep}) is calculated with the standard deviation (σ), as shown in the following:

$$\sigma = \sqrt{\frac{\sum_{i=1}^{n} \left(m_{dep} - \overline{m}_{dep}\right)^{2}}{n-1}} \tag{4}$$

$$\Delta \overline{m}_{dep} = \frac{t_{\alpha} \sigma}{\sqrt{n}} \tag{5}$$

where m_{dep} represents the wax deposition mass for each measurement, n is the number of measurements, and ta is the upper quantile of the t-distribution with a confidence interval of 0.95, where t_a =2.776 for n = 5.

Table 2 presents the deposition mass on PS from the repeated tests. It can be observed from the table that the standard deviation of the deposition mass for the PS from the five tests is 0.0057g. Meanwhile, the measurement uncertainty for the deposition mass is 0.0072g, with relative uncertainty of 5.36%. For the deposition on the surface of the model, the random errors in the entire experimental system are relatively small.

Table 2 Test results of PS deposition mass

i	m_{dep} / g	$ar{m}_{dep}$ /g	σ /g	$\Delta \overline{m}_{dep}^{}/{ extsf{g}}$	$rac{\Delta \overline{m}_{dep}}{\overline{m}_{dep}}$ / %
1	0.130				
2	0.127	0.134	0.0057	0.0072	5.36
3	0.136				

4	0.138		
5	0.141		

3.2 The depositing for different AOAs

In this section, the cylindrical model is selected for studying the influence of the AOA on the particle deposition characteristics. The deposition tests are conducted with AOA of 0°, -5°, and -15°, and the other parameters are listed in Table 1. Figure 7 illustrates the distribution of PS deposition on the cylindrical model at different AOAs. The deposition is primarily concentrated downstream of the holes and the deposition distribution patterns are almost the same for different AOAs. When α=0°, there is still some wax deposition upstream of the holes, however, as the AOA increases, the deposition thickness downstream of the holes increases while the deposition upstream of the holes decreases. When α =-15°, there is almost no deposition in areas other than downstream of the holes on the PS. As the AOA increases, more deposition forms, the "ridge" downstream of the holes becomes more distinct, and the "lump" wax deposits grow larger. From Figure 7, it is evident that the primary deposition zone progressively widens from the vicinity of the holes to encompass the entire rear surface as the angle of attack (AOA) increases. This is due to the windward area expansion with AOA increasing and more wax could be captured and deposited on the rear of the PS. The deposition rates on the PS of the cylindrical, models at different AOAs are shown in Figure 8. It is evident that as the AOA increases, the deposition rates on the PS exhibit an increasing trend. When $\alpha=0^{\circ}$, the deposition rate on the PS of the cylindrical model is approximately 0.30%. When α=-5°, the deposition rate increases to around 0.48%, namely a relative increase of about 60%. Further increasing the AOA to -15° results in a deposition rate of approximately 0.66%, indicating a relative increase of about 110% compared to 0°.

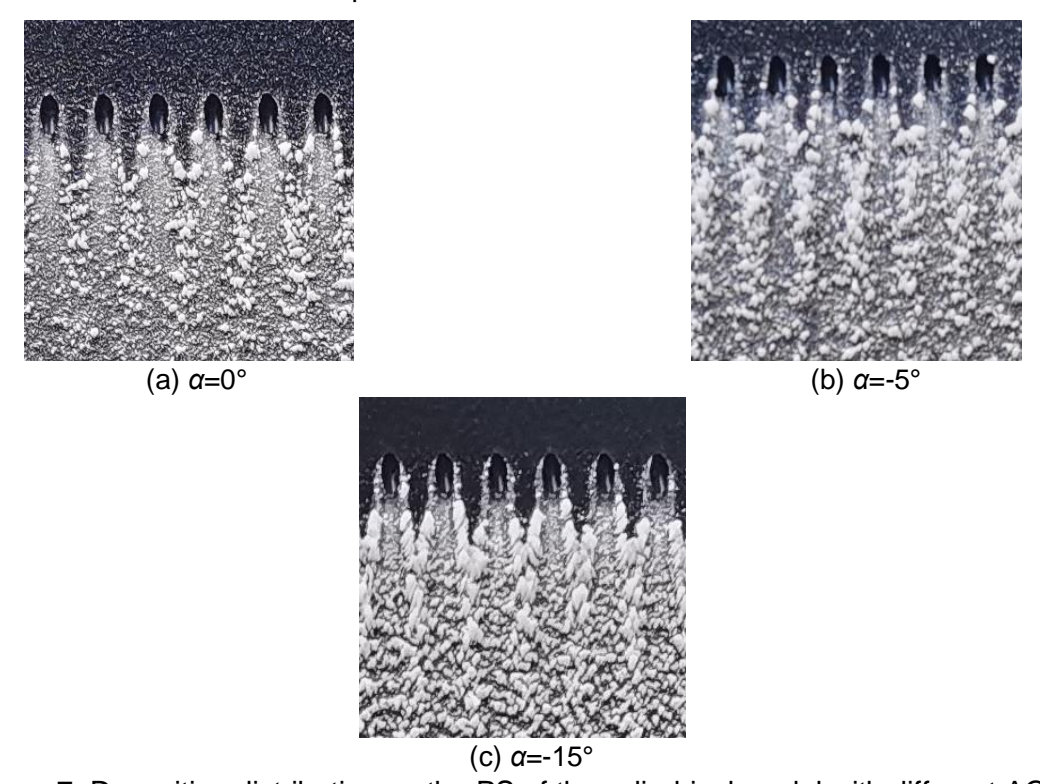


Figure 7-Deposition distribution on the PS of the cylindrical model with different AOAs

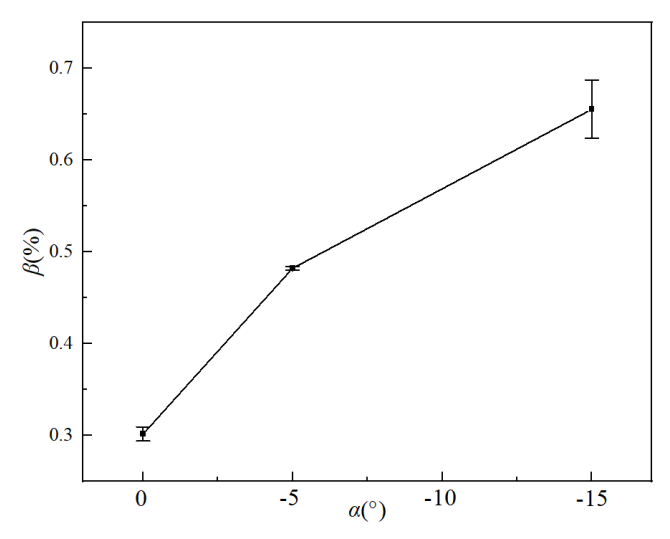
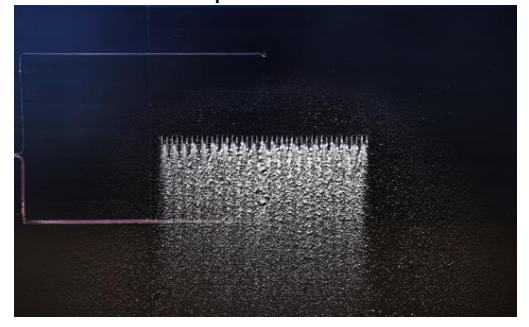


Figure 8-Deposition rate on the PS with different AOAs

3.3 The effect of different film-cooling hole shapes on the depositing

The deposition is primarily concentrated downstream of the holes and the deposition distribution patterns are almost the same for different AOAs. Therefore, the angle of attack is selected as -5° for the investigation on the effect of the different hole shapes on the deposition. Figure 9 shows the distribution of deposition on the PS with different film-cooling hole shapes and a localized magnified view of the PS deposition is presented for ease of observation. It is evident that the deposition distribution on the PS of all models is mainly concentrated downstream of the film-cooling holes, and the most deposition forms on the PS of the cylindrical model. There is "lump" accumulation on the PS of all models and a "band" distribution that continues to the tail of the model. The "lump" accumulation of the cylindrical model is maximum, while the deposition distribution of the fan-shaped model and RTSH model are more uniform.





(a) Deposition distribution on the PS of the cylindrical model





(b) Deposition distribution on the PS of the fan-shaped model





(c) Deposition distribution on the PS of the RTSH model

Figure 9–Deposition distribution on the PS of the models with different film-cooling hole shapes

The phenomenon shown in Figure 9 could be illustrated by the effective blow ratio. In this study, all tests were conducted with a consistent blow ratio of 3.0, as documented in Table 1. The blow ratios for different film cooling hole shapes are defined by using the film cooling air density and velocity at the minimum throat area of the film-cooling hole. In this case, although the blow ratios for different models are the same, the effective blow ratios at the film-cooling hole exits for different hole shapes are different, inducing different flow structures near the film-cooling holes. According to the dimensions of the holes shown in Figure 3, the fan-shaped hole generates the lowest effective blow ratio at its exit since it has the maximum cross area 11.30mm² at its exit. Similarly, the cylindrical hole generates the largest effective blow ratio at its exit. This means that weaker secondary flow forms near the fan-shaped hole than the cylindrical hole, accordingly bringing less particles onto the surface of the model due to the good flow tracking of the particles and producing less deposition on the fan-shaped model. For the same reason, less deposition forms on the RTSH model than the cylindrical model. On the other hand, the fan-shaped and RTSH holes feature a broader transverse width, leading to more uniform flow in the spanwise direction and accordingly more uniform deposition distribution on the PS, compared to the cylindrical hole. In addition, the weaker secondary flows due to the lower effective blow ratio for the RTSH and fan-shaped holes make the flow reattach at a more upstream location. Therefore, for the RTSH and fan-shaped models, less particles could be taken onto the surface and the deposition near the tail of the models become much less than those of the cylindrical model.

The deposition rate for different models is also discussed. Figure 10 shows the changes in deposition rate on the PS of the models with different film-cooling hole shapes. The error bars are also shown in Figure 10. The deposition amount of wax on the PS was measured by high-precision balance. The deposition rates of the PS for the cylindrical, fan-shaped and RTSH model are 0.48%, 0.085% and 0.10%, respectively. The deposition rate of RTSH model is 79 % lower than that of the cylindrical model, and the deposition rate of the fan-shaped model is 83 % lower than that of the cylindrical model. It indicates that the change of film-cooling hole shape can effectively reduce the deposition of wax, which is consistent with the trend illustrated in figures 9 (a) \sim (c). The deposition amount comparison among the three models could be attributed to the flow structure due to different effective blow ratios at the exits for the different shapes of film-cooling holes, as illustrated above.

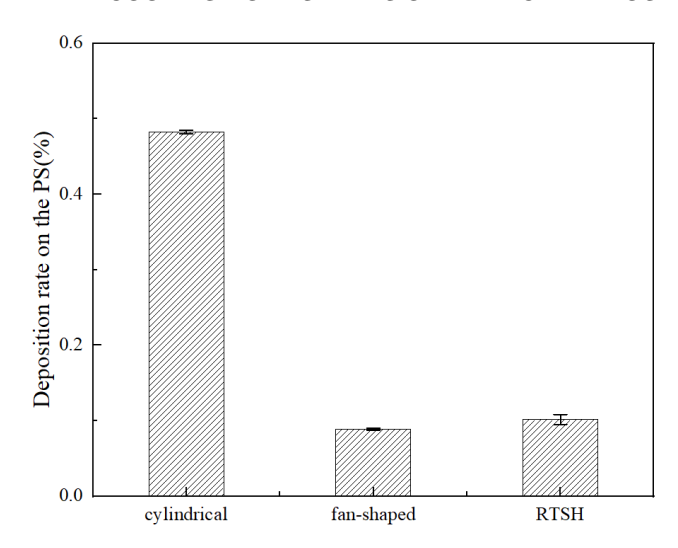


Figure 10-Deposition rate on the PS with different film-cooling hole shapes

3.4 The effect of different film-cooling hole shapes on the cooling efficiency

The PS temperature distributions of different models are measured by using an infrared camera to calculate the cooling efficiencies. Figure 11 shows the PS cooling efficiency downstream of the film-cooling holes with different film-cooling hole shapes, where X/D and Y/D represent the ratios of the distances in the X and Y directions to the diameter D (2mm) of the cylindrical hole, with X indicating the streamwise direction and Y indicating the spanwise direction of the PS. It is evident that the cooling efficiency of cylindrical model is lower than other models, indicating weak cooling performance. At X/D=6, the cooling efficiency of the RTSH model downstream of the film hole is increased by a maximum of 26 % (note that this value is not relative value), and the cooling efficiency of the fan-shaped model is increased by a maximum of 19 %.

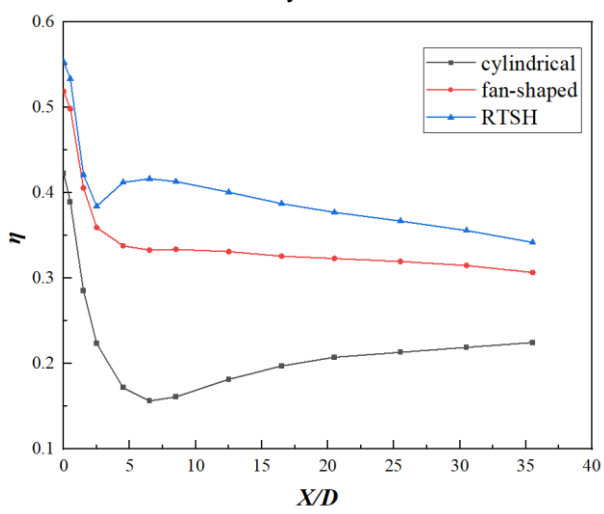
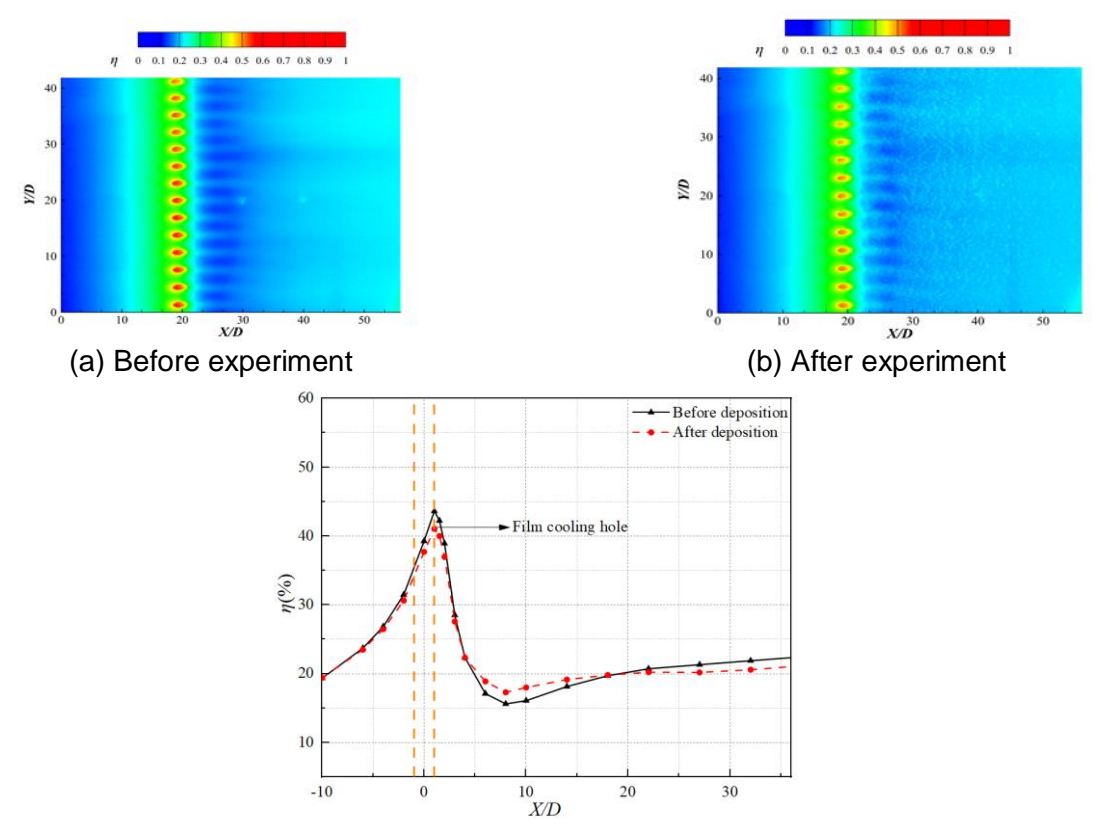


Figure 11–cooling efficiency downstream of the film-cooling holes with different film-cooling hole shapes

Figure 12 is the cooling efficiency comparison of the cylindrical model before and after the experiment. It is evident that the high temperature zone in Figure 12(a) disappears after deposition, and the film-cooling efficiency is increased. Figure 12(c) gives the comparison of the average cooling efficiency before and after deposition. It can be seen that the spanwise average cooling efficiency upstream of the film-cooling holes does not change significantly, because there is less wax deposition in this area. At $2D \sim 15D$ after the film-cooling holes, the average cooling efficiency in the spanwise direction is improved after the experiment, and the maximum is increased by about 1.8% at X/D = 6. From 15D to the tail, the average efficiency in the spanwise direction decreases

by about 1.3% after the deposition.

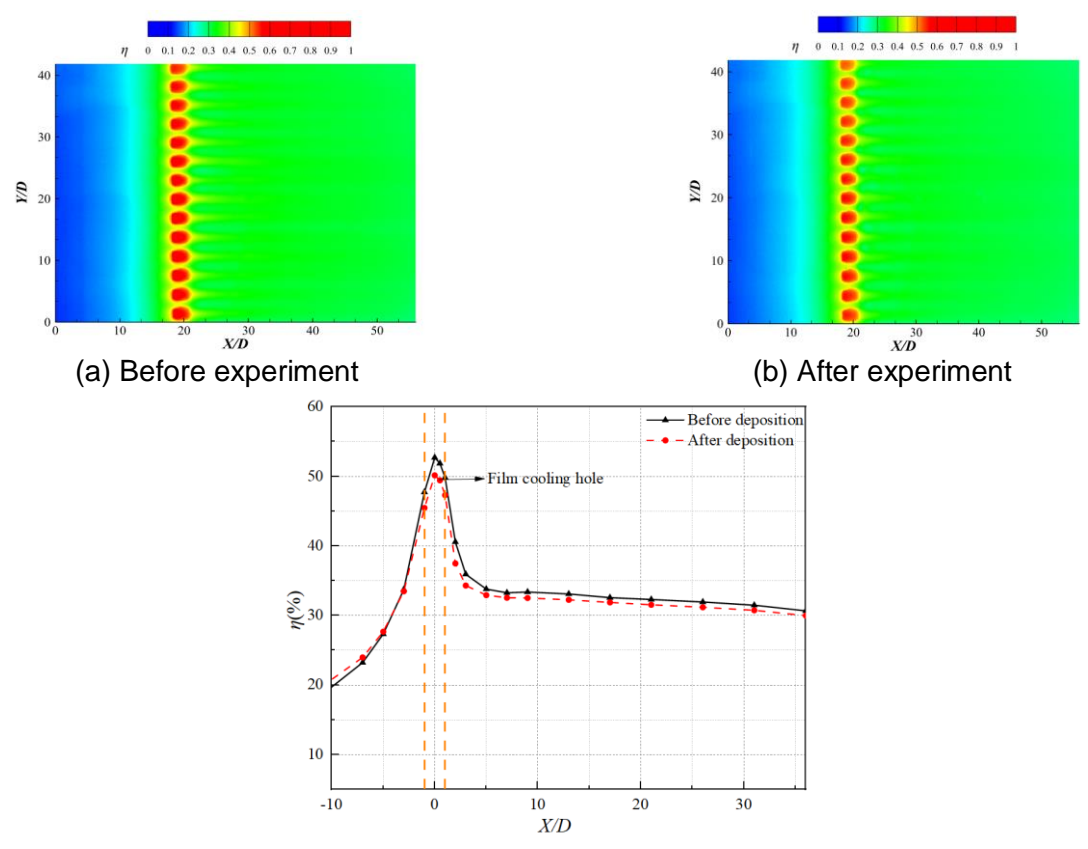


(c) Cooling efficiency before and after deposition of the Cylindrical model Figure 12–Distribution of cooling effectiveness before and after deposition of cylindrical model

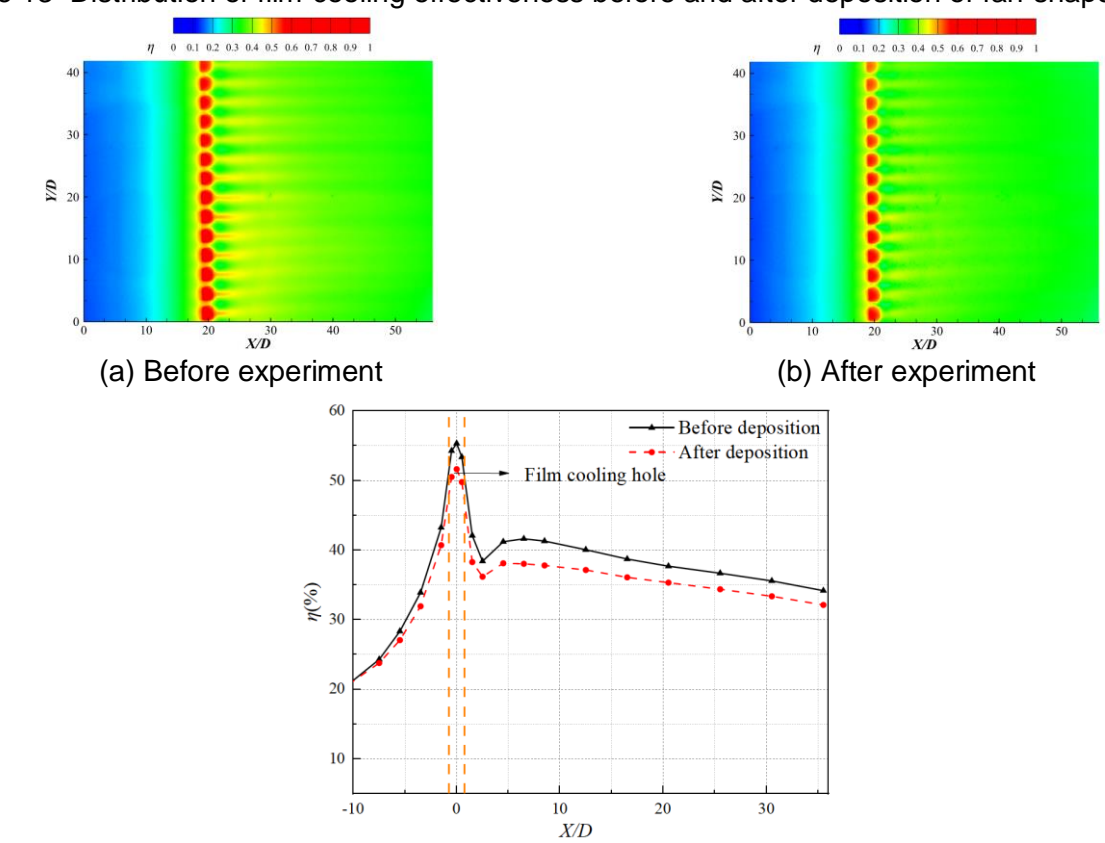
Figures 13-14 are the cooling efficiency distribution of the other two models before and after experiment. It is evident that, comparing the cooling efficiency before and after the experiment of each model, the average cooling efficiency of the RTSH hole is reduced by about 2.2%, and the fan-shape film hole structure has no obvious change.

It can be seen by comparing Figures 12-13 that the fan-shaped and RTSH holes could generate more uniform temperature distribution than the cylindrical holes. This could also be attributed to the fact that the second flow is weaker due to the smaller effective blow ratios at the hole exits for the fan-shaped and RTSH models, preventing more mainstream flow with higher temperature from heating the models, as discussed above. The more uniform particles deposition forms on the PS of the fan-shaped and RTSH models and accordingly could not change the cooling effectiveness obviously. However, the more uniform temperature distribution downstream of the PS may be another reason for the more uniform deposition.

It seems that the fan-shaped and RTSH holes are preferable to the cylindrical hole no matter from the aspect of reducing deposition or cooling performance according the results in this paper. However, it should be noted that the models are basically plate and the blow ratio is kept as 3.0, furthermore, the experiments were conducted at the mainstream temperature only a little higher than ambient temperature. Therefore, further studies should be conducted to investigate whether the fan-shaped and RTSH holes have the good performances both in reducing deposition and cooling in other situations and at high temperature close to the typical mainstream temperature before turbine vanes.



(c) Cooling efficiency before and after deposition of the fan-shaped model Figure 13–Distribution of film-cooling effectiveness before and after deposition of fan-shaped mode



(c) Cooling efficiency before and after deposition of the RTSH model Figure 14–Distribution of film-cooling effectiveness before and after deposition of RTSH model

4. CONCLUSIONS

This paper investigates the influence of the film-cooling hole shape on the particle deposition by the tests with the plate models configured with three types of film-cooling hole conducted on the ambient temperature deposition platform. The three types of film-cooling holes are cylindrical, fanshaped and RTSH hole. In addition, the deposition characteristic at different AOAs is studied by using the cylindrical model. The main conclusions are as follow:

- (1) Under different angles of attack, the deposition rates on the pressure surface increase with the increase of angle of attack. As the angle of attack increases from 0° to -15°, the relative increase in the deposition rate on the pressure surface of the cylindrical model is 110%, however, the deposition distribution does not change much.
- (2) The deposition distribution on the PS is mainly concentrated downstream of the film-cooling hole for all models, among which the cylindrical model is deposited most, with obvious "band" distribution and "lump" accumulation. There is less deposition downstream of the film-cooling hole in other models, and the wax deposition at the tail does not continue to form obvious "band" distribution, and there is a small amount of wax "lump" accumulation.
- (3) The deposition rate on the PS of the cylindrical model is 0.48 %, the deposition rate of the RTSH model is relatively reduced by 79%, and the deposition rate on the PS of the fan-shaped model is relatively reduced by about 83%, it indicates that the change of the hole type can effectively reduce the deposition.
- (4) The cooling efficiency of RTSH model and fan-shaped model is better than cylindrical model. The fan-shaped model is improved by up to 16% (not relative value), and the RTSH model is improved by up to 29%.
- (5) Due to the large amount of deposition on the PS of the cylindrical model, the cooling efficiency changes most obviously after the deposition formation, while the cooling efficiency of other models before and after deposition formation is not significantly different.

Contact Author Email Address

Mail to: zgliu@nwpu.edu.cn

Copyright Statement

The authors confirm that they, and/or their company or organization, hold copyright on all of the original material included in this paper. The authors also confirm that they have obtained permission, from the copyright holder of any third party material included in this paper, to publish it as part of their paper. The authors confirm that they give permission, or have obtained permission from the copyright holder of this paper, for the publication and distribution of this paper as part of the ICAS proceedings or as individual off-prints from the proceedings.

References

AN EXPERIMENTAL SIMULATION ON THE INFLUENCE OF DIFFERENT FILM COOLING HOLE SHAPES ON PARTICLE DEPOSITION ON TURBINE VANE

- [1] Jensen J W, Squire S W, Bons J P, et al. Simulated land-based turbine deposits generated in an accelerated deposition facility. *American Society of Mechanical Engineers*, Vol. 127, No. 3, pp 462-470, 2004.
- [2] Smith C, Barker B, Clum C, et al. Deposition in a turbine cascade with combusting flow. *Proceedings of the ASME Turbo Expo 2010: Power for Land, Sea, and Air*, UK, Vol.4, pp 743-751, 2010.
- [3] Prenter R, Ameri A, Bons J P. Deposition on a cooled nozzle guide vane with non-uniform inlet temperatures. *Journal of Turbomachinery*, Vol. 138, No. 10, pp 101005.1-101005.11 2016.
- [4] Liu Z G, Zhang F, Liu Z X, et al. An experimental study of the effects of different transverse trenches on deposition on a turbine vane with film-cooling at high temperature. *Aerospace Science and technology*, Vol. 107, No. Dec, pp 106340.1-106340.10, 2020.
- [5] Zhang F, Liu Z X, Liu Z G, et al. Experimental study of sand particle deposition on a film-cooled turbine blade at different gas temperatures and angles of attack. *Energies*, Vol. 13, No. 4, pp 1-19, 2020.
- [6] Lawson S A, Lynch S P, Thole K A, et al. Simulations of multiphase particle deposition on a non-axisymmetric contoured endwall with film-cooling. *Journal of Turbomachinery*, Vol. 135, No. 3, pp 031032.1-031032.10, 2013.
- [7] Lawson S A, Thole K A, Okita Y, et al. Simulations of multi-phase particle deposition on a showerhead with staggered film-cooling holes. *Journal of Turbomachinery*, Vol. 134, No. 5, pp 051041.1-:051041.12, 2012.
- [8] Lawson S A, Thole K A. Simulations of multi-phase particle deposition on endwall film cooling. *Journal of Turbomachinery*, Vol. 134, No. 1, pp 011003.1-011003.11, 2012.
- [9] Albert J E, Bogard D G. Experimental simulation of contaminant deposition on a film cooled turbine airfoil leading edge. *Journal of Turbomachinery*, Vol. 134, No. 5, pp 051014.1-051014.10, 2012.
- [10] Albert J E, Bogard D G. Experimental simulation of contaminant deposition on a film cooled turbine vane pressure side with a trench [J]. Journal of Turbomachinery, Vol. 135, No. 9, pp 051008.1-051008.11, 2013.
- [11] Davidson F T, Kistenmacher D A, Bogard D G. A study of deposition on a turbine vane with a thermal barrier coating and various film cooling geometries. *Journal of Turbomachinery*, Vol. 136, No. 4, pp 1769-1780, 2012.
- [12] Liu Z G, Liu Z X, Zhang F, et al. An experimental study on the effects of a film cooling configuration and mainstream temperature on depositing. *Journal of Thermal Science*, Vol. 28, No. 2, pp 360-369, 2019.
- [13] Liu Z G, Liu Z X, Zhang F, et al. An experimental study of the effects of different transverse trenches on depositing and temperature on a plate with film cooling holes. *Aerospace Science and technology*, Vol. May, No. 88, pp 40-50, 2019.
- [14]Yang X J, Cui M H, Liu Z G. Experimental study on particle deposition of plate surface with film cooling. *Journal of propulsion technology*, Vol. 39, No. 6, pp 1323-1330, 2018.
- [15] Yang X J, Yu T H, Cui M H, et al. Experiment on gas film cooling efficiency in environment of deposition. *Journal of Beijing University of Aeronautics and Astronautics*, Vol. 45, No. 8, pp 1681-1690, 2019.